Pneumatochemical Impedance Spectroscopy. 2. Dynamics of Hydrogen Sorption by Metals

Pierre Millet*

Laboratoire de Chimie Inorganique, Université Paris Sud, bâtiment 420, 91405 Orsay cedex, France

Received: June 21, 2005; In Final Form: October 1, 2005

In this paper, pneumatochemical impedance spectroscopy is used to analyze multistep reaction mechanisms such as those observed in solid solution domains of $LaNi_5-H_2(g)$ systems. It is shown that hydrogen sorption is a two-step mechanism including (i) dissociative surface chemisorption of molecular hydrogen and (ii) atomic hydrogen bulk transport by diffusion. Data fitting of experimental transfer functions with model equations yields the value of the kinetic parameter associated with each individual reaction step, i.e., surface sorption resistances and hydrogen bulk diffusion coefficients. The technique is used to follow the activation procedure of the sample as well as the degradation of sorption properties in oxygen-containing hydrogen atmospheres. A decrease in sorption kinetics is attributed to surface oxidation, whereas bulk properties remain unchanged. The perspectives offered by the technique which potentially can be used to optimize surface and bulk composition of IMC for increased sorption rates are discussed.

1. Introduction

Kinetic investigation of intermetallic compound (IMC)$-H_2$-(g) systems requires particular attention. Experimentally, reaction rate measurements are commonly made by measuring the transient hydrogen pressure in a closed system with constant volume. This is the so-called Sievert's method, and the experimental setup used to perform such measurements is often referred to as a Sievert's-type gas distribution apparatus (SGDA). In early research works on these systems, many rate observations were those of heat transfer limitations.[1,2] The heat released in the powdered sample during hydrogen absorption may lead to significant temperature changes and nonisothermal observations, because of the poor thermal conductivity of the reacting bed. The problem can be solved by using a needle valve which acts as a gas flow regulator: hydrogen is transferred isothermally from the reference volume chamber to the reaction chamber under laminar conditions.[3] The reaction scheme associated with isothermal hydrogen absorption/desorption reactions is reasonably known. According to Martin et al.,[4] the overall reaction contains up to five elementary and sequential steps including (i) van der Waals-type weak physisorption of dihydrogen molecules from the gas phase onto the surface of the IMC, (ii) surface dissociation of dihydrogen molecules and chemisorption leading to the formation of adsorbed hydrogen adatoms, (iii) transfer of adatoms from the surface to the subsurface, (iv) atomic hydrogen transport from the subsurface to the bulk sample by diffusion involving either interstitial or vacancy mechanism, and (v), in the two-phase domain, hydride formation at the expanding hydride−core/metal interface. The usual method to analyze kinetics is to fit the time-dependent transformed fraction $\alpha(t)$ with various analytical rate expressions, so as to identify the rate-determining step (rds) of the reaction, the other steps being considered at equilibrium.[5,6] These models lead to kinetic rate laws which in general agree with experimental data, but sometimes only on limited time intervals. It is generally admitted that changes in rds may occur during absorption and that only numerical solutions can be expected when considering the total reaction scheme.[7] Curiously, the same situation prevailed more than 30 years ago.[8] Therefore, there is still a need to analyze multistep reaction schemes with time-dependent rds. Such analysis is routine in electrochemistry using electrochemical impedance spectroscopy (EIS). Instead of modeling transient current densities produced by given potential perturbations (time domain), the transfer function of the system is measured (Fourier or frequency domain) using either harmonic[9] or polychromatic perturbations.[10] Transfer functions unambiguously characterize reaction mechanisms and give access to the rate parameter associated with each step. In favorable cases, the signature of each step appears at different frequencies, providing direct evidence of the detailed mechanism. By making an analogy between pressure and electric potential on one hand and gas flow and electric current on the other hand, it is possible to define the basic principles of pneumatochemical impedance spectroscopy (PIS), which is the direct transposition of EIS to solid−gas reactions. The principles and applications of this spectroscopy are discussed in this paper, which is organized in two parts. In the first part, a description of the basic principles of PIS analysis restricted to gas transfer dynamics (with no hydriding reaction) is presented. The general characteristics of the pneumatic components used in SGDA are obtained by measurement-supported modeling of transient pressure and gas flow signals, both in the time and frequency domains. The conditions under which the needle valve acts as pneumatic resistances and the volumic chambers act as pneumatic capacitors are discussed. In the second part, an electrical analogy is developed to model gas transfer dynamics and absorption phenomena using SGDA. Experimental transfer functions of IMC$-H_2$(g) systems are obtained in relation with absorption/desorption isotherms in solid solution domains. Model transfer functions are derived and compared to experimental data. The interest of the method for studying IMC$-H_2$(g) systems, with regard to absorption/desorption rate improvement as well as material degradation during cycling, is discussed.

* Phone: 33-1.6915.4812. Fax: 33-1.6915.4754. E-mail: pierre.millet@icmo.u-psud.fr.

10.1021/jp053351e CCC: $30.25
Published on Web 11/24/2005

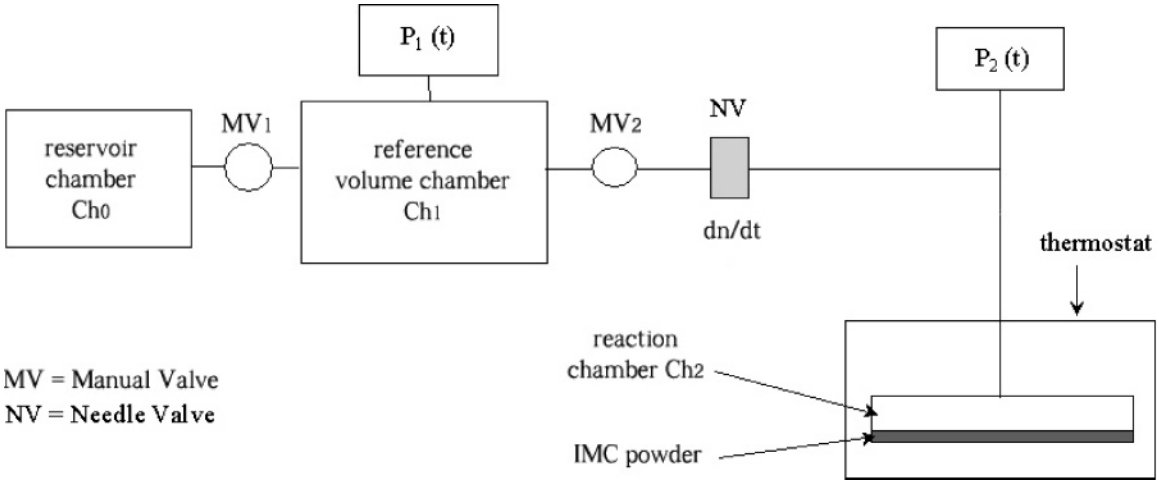

Figure 1. Schematic representation of the SGDA used to analyze the dynamics of H_2 sorption by metals and IMC.

2. IMC−H_2(g) Systems and the Theory of Linear and Time Invariant Systems

Let us consider IMC−H_2(g) systems in which hydrogen is exchanged between the gas phase and the IMC, along a multistep reaction path. As discussed in part 1 of this paper using the theory of systems, mechanism information can be obtained by analyzing any given pair $\{i(t);o(t)\}$ where $i(t)$ = pressure(t) and denotes the input pressure transient applied to the IMC−H_2(g) system and $o(t) = dn/dt(t)$ is the corresponding mass flow response. Such analysis can be performed either in the time or in the frequency (Fourier) domain. However, there is an immediat benefit at working in the frequency domain: whereas the relation between $i(t)$ and $o(t)$ is a convolution in the time domain, this is a simple algebraic product in the frequency domain. Thus, the transfer function of the system can be obtained easily at the cost of two numerical Fourier transformations. Another benefit is that the global transfer function of a multistep reaction path is simply an algebraic combination of the transfer function of each individual step. Modeling is therefore significantly simplified. The problem is thus to obtain experimental and model pneumatochemical transfer functions. In electrical or electrochemical systems, experimental impedance is measured using an harmonic analyzer: the complex impedance of the system (voltage to current amplitude modulation and phase shift) is measured frequency after frequency over the frequency domain of interest, using monochromatic perturbations. This cannot be done for solid−gas reactions. There are experimental limitations. Gray et al. have reported on this harmonic method for IMC−H_2(g) systems.[11] They used monochromatic pressure modulations generated by thermal heating and measured the corresponding weight changes using a microbalance. A limitation comes from the frequency domain over which measurements can be done. A maximum value of 0.1 Hz is reported in ref 11 because of thermal inertia in the harmonic pressure generator. This value may be insufficient for studying fast surface processes such as physisorption and surface dissociation. Secondly, there are physical limitations. Most IMC−H_2(g) systems exhibit a significant pressure hysteresis. In two-phase ($\alpha-\beta$) domains, absorption and desorption pressure plateaus on the isotherms are significantly different. This is synonymous with irreversibility and nonlinearity, and the theory of linear and time-invariant systems presented in the first part of this paper does not apply: a harmonic pressure input will generate a nonharmonic mass flow response. The Fourier transform (FT) of this nonharmonic response will contain several frequencies (the main frequency of the input perturbation and additional harmonics) and the frequency-to-frequency relationship leading to the transfer function will not be satisfied. It should be noted that hysteresis exhibited by metal hydrides is static in nature: it cannot be reduced experimentally.[12] By strictly monitoring the physical parameters used during experiments with SGDA (mainly the driving force and the duration of elementary gas transfers), it is possible to obtain regularly shaped isotherm envelopes[13] and to minimize the amplitude of hysteresis but not to eliminate it. An isotherm is a succession of nonequilibrium states in the pressure−composition domain. This fundamental problem which proscribes the use of harmonic input functions can be bypassed by applying nonharmonic perturbations. In particular, monotonic perturbations (time functions with strictly positive first-order time derivative for absorption and strictly negative first-order time derivative for desorption) can be advantageously used. In such cases, the system is said to be linear by part since there are no back and forth displacements along nonreversible thermodynamic paths. In other words, it is possible to perform Fourier-domain analysis of kinetics in IMC−H_2(g) systems using classical SGDAs. Experimental transfer functions are obtained from the convolution equation

$$\mathrm{FT}[i(t)*h(t)] = \mathrm{FT}[i(t)]\ \mathrm{FT}[h(t)] = \mathrm{FT}[o(t)] \qquad (2.1)$$

where $h(t)$ is the impulse response of the system and $\mathrm{FT}[h(t)] = H(f)$ is the unknown transfer function, as discussed in part 1.

A time-dependent nonharmonic perturbation is used as input, and the related output is synchronically sampled. Each individual signal $i(t)$ and $o(t)$ is then numerically Fourier transformed (using either fast Fourier transform (FFT) algorithms[14,15] or discrete Fourier transformation (DFT) by direct integration). The complex ratio of the two FTs is computed over the frequency domain of interest, and this yields the desired transfer function. The use of the convolution eq 2.1 is restricted to perturbation signals having nonzero FTs at the frequencies of interest, and this has to be checked.

3. Experimental Section

The experimental SGDA used to analyze the dynamics of IMC−H_2(g) systems has been described in detail in part 1. A simplified and functional drawing of the equipment used to perform sorption experiments is shown in Figure 1. During absorption, hydrogen is transferred from the reference chamber Ch_1 to the reaction chamber Ch_2 where reaction with the powdered IMC takes place. The needle valve (NV) acts as a

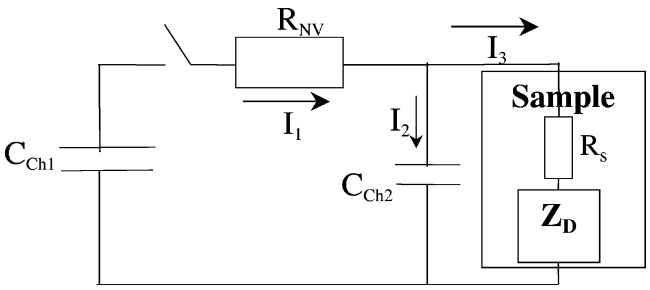

Figure 2. Electrical equivalent circuit of the experimental setup of Figure 1. The transfer function of the sample consists of a surface resistance R_s in series connection with a diffusion impedance Z_D.

TABLE 1: Electrical−Pneumatical Equivalences

electrical	pneumatical
electric potential $E \equiv q/C$ (V)	pressure P (Pa)
electric current I (A)	molar gas flow dn/dt (mol·s^{-1})
electric capacitance C (F)	pneumatic capacitance V/RT (mol·Pa^{-1})
electric charge q (Cb)	number of gaseous moles (PV/RT)
electric resistance (Ω)	pneumatic resistance $R_{NV} = RT/K_v P_1^0 \equiv$ Pa·s·mol^{-1}

gas flow regulator to avoid convective and nonisothermal gas transfers. Transient pressure signals $P_1(t)$ and $P_2(t)$ are sampled all along the transfer process and provide raw data for PIS analysis of sorption mechanisms.

4. Electrical Analogies

As shown in part 1, the needle valve (NV) acts as a pneumatic resistance (R_{NV}) and the volumic chambers act as pneumatic capacitors (C_{Ch_1} and C_{Ch_2}). Therefore, the experimental setup of Figure 1 can be modeled using the electrical equivalent circuit of Figure 2.

In the electrical analogy, each component of the pneumatic circuit offers a linear response and the equivalences given in Table 1 can be used.

In a typical experiment, hydrogen stored in the reference volume chamber Ch_1 is transferred to the reaction chamber Ch_2 where it either reacts (I_3) with the IMC (through a two-step serie mechanism) or accumulates (I_2) in the free volume part of the reaction chamber.

5. Pneumatochemical Impedances Obtained in Solid Solution Domains

5.1. Measure of Raw Kinetic Data. The isotherm of $LaNi_5$−H_2(g) measured at 298 K in the solid solution domain is shown in Figure 3. Each equilibrium point was obtained by transferring hydrogen amounts from Ch_1 to Ch_2 ($\Delta H/M \approx 0.06$).

Raw isothermal kinetic information is obtained by sampling transient pressures $P_1(t)$ and $P_2(t)$ during gas transfers. Assuming that hydrogen behaves ideally (this is justified for systems with plateau pressures at 2 bar as those considered in the present work), the transient hydrogen molar flow dn/dt is calculated from $P_1(t)$ using the perfect gas law

$$\frac{dn}{dt}(t) = \frac{V_{Ch_1}}{RT}\frac{dP_1}{dt}(t) \qquad (5.1)$$

Figure 4 shows experimental results obtained during gas transfer from H/M = 0.0 to 0.065 in Figure 3.

5.2. Computation of Experimental Pneumatochemical Transfer Functions. The experimental transfer function of the $LaNi_5$−H_2(g) system is obtained using (2.1). Discretely sampled transient $P_2(t)$ and dn/d$t(t)$ signals are numerically Fourier transformed, and the complex ratio is plotted in Nyquist

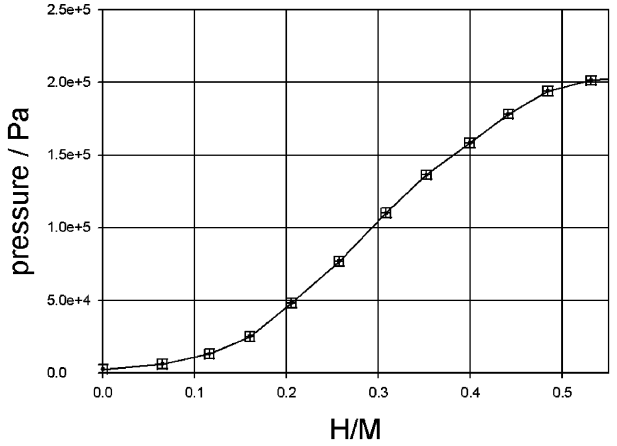

Figure 3. Experimental isotherm of $LaNi_5$−H_2(g) measured at 298 K in the solid solution domain.

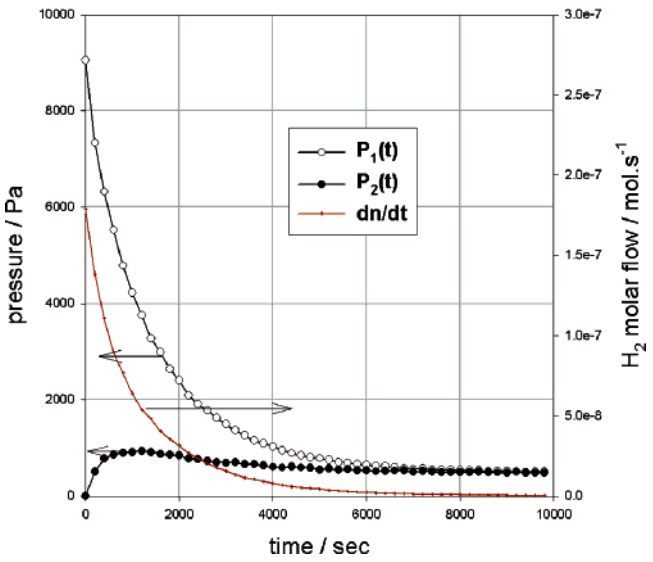

Figure 4. Experimental $P_1(t)$ and $P_2(t)$ mesured for $LaNi_5$ at 298 K and H/M = 0.065. Gas flow is calculated from $P_1(t)$ using (5.1); $m(LaNi_5) = 2.374$ g.

coordinates as a function of frequency. Figure 5 shows the experimental impedance diagram obtained from the transients of Figure 4.

Typically, mechanism information is spread over a domain of frequencies ranging from 10^{-2} mHz at low frequency (LF) up to 1 Hz at high frequency (HF). The HF limit obtained in Figure 5 is {0;0} and not {R_{NV};0} because this is the graph of $Z_2(\omega) = P_2(\omega)/[dn/dt(\omega)]$ (where $P_2(t)$ is measured after the needle valve) and not $Z_1(\omega) = P_1(\omega)/[dn/dt(\omega)]$.

5.3. Modeling. The mechanism of hydrogen absorption in solid solution domains has been extensively studied in electrochemistry. According to ref 16, the cathodic hydrogen evolution reaction (her) from acidic aqueous solutions follows two consecutive steps: (i) the discharge of hydrated protons (a) and (ii) dihydrogen evolution by either chemical (b) or electrochemical (c) desorption

$$H^+ + M + e^- \rightarrow MH_{ad} \qquad (a)$$

$$MH_{ad} + MH_{ad} \rightarrow H_2 + 2M \qquad (b)$$

$$H^+ + MH_{ad} + e^- \rightarrow H_2 + M \qquad (c)$$

where M is a metallic site and MH_{ad} is a hydrogen atom adsorbed on the metal surface.

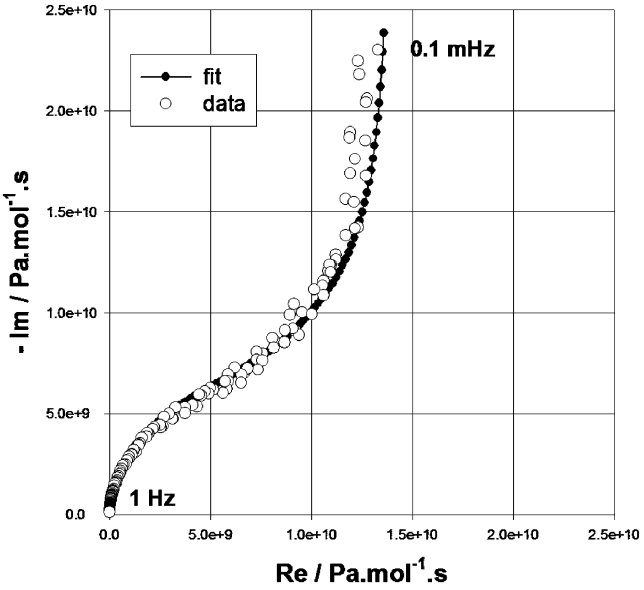

Figure 5. Nyquist plots of the transfer function of $LaNi_5-H_2(g)$ at 298 K and H/M = 0.065: measured (○) from the experiment of Figure 4 using (2.1) and calculated (●) using (5.2).

However, metals absorb hydrogen to some extent and the hydrogen absorption reaction (har) provides an alternative reaction path (d) in parallel to steps (b) or (c):

$$MH_{ad} \rightarrow M + H_{ab} \qquad \text{(d)}$$

where H_{ab} is a hydrogen atom absorbed in the metal subsurface. Absorption proceeds by diffusion-controlled mass transport to bulk regions (e)

$$H_{ab}{}^{x=0} \rightarrow H_{ab}{}^{bulk} \qquad \text{(e)}$$

In two-phase domains, a further step of hydride precipitation occurs.

When hydrogen absorption occurs from the gas phase, only the surface reaction step differs. Dihydrogen chemisorption occurs in one (f) or two (g, h) steps

$$H_2(g) + 2M \rightarrow 2MH_{ad} \qquad \text{(f)}$$

$$H_2(g) + 2M \rightarrow MH_2 \qquad \text{(g)}$$

$$MH_2 \rightarrow 2MH_{ad} \qquad \text{(h)}$$

By considering a reaction path based on steps f and e and neglecting step d, the pneumatochemical transfer function of the system $Z(\omega)$ is that of the electrical analogy of Figure 2: series connection of a pulsation-independent surface resistance, R_s, and a diffusion impedance, $Z_D(\omega)$, in parallel with the capacitance of the reaction chamber

$$Z(\omega) = R_{NV} + \left[\left(\frac{1}{jC_{Ch_2}\omega + \left(\frac{1}{R_s + Z_D}\right)}\right)\right] \qquad (5.2)$$

where R_{NV} is the pneumatic resistance of the needle valve, C_{Ch_2} is the capacitance of the reaction chamber Ch_2, R_s is the surface resistance associated with the chemisorption process (step f), and Z_D (step e) is the classical diffusion impedance[17,18] corrected[19] to account for solid−gas reactions. Considering the powder morphology of the sorbing IMC, it is logical to choose for Z_D the analytical solution obtained for diffusion in spherical coordinates

$$Z_D{}^{sphere}(\omega) = \frac{r}{D}\frac{\partial P_{H_2}}{\partial C_H}\frac{1}{[u\coth(u) - 1]} = R_D{}^{sphere}\frac{1}{[u\coth(u) - 1]} \qquad (5.3)$$

where

$$R_D{}^{sphere} = \frac{r}{D}\frac{\partial P_{H_2}}{\partial C_H}$$

$$u = \sqrt{\frac{j\omega r^2}{D}} \qquad (5.4)$$

r is the radius of the sorbing particle, D is hydrogen diffusion coefficient, $\partial P_{H_2}/\partial C_H$ is the slope of the isotherm (Figure 3) at the measurement point, and ω is the pulsation in rad·s^{-1}. In eq 5.2, R_s is a real number independent of the pulsation ω. In eq 5.3, the real and imaginaty parts of $Z_D(\omega)$ can be calculated separately using

$$u = \sqrt{\frac{j\omega r^2}{D}} = \sqrt{\frac{\omega r^2}{2D}} + j\sqrt{\frac{\omega r^2}{2D}} \qquad (5.5)$$

$$\coth u = \frac{e^u + e^{-u}}{e^u - e^{-u}} \qquad (5.6)$$

and Euler's formula

$$e^{j(\omega r^2/2D)^{1/2}} = \cos\sqrt{\frac{\omega r^2}{2D}} + j\sin\sqrt{\frac{\omega r^2}{2D}} \qquad (5.7)$$

The fitting of experimental data obtained on powdered samples with eq 5.3 yields an averaged value of D, function of the particle size distribution.

5.4. Data Fitting and Discussion. The experimental transfer function of Figure 5 was fitted with eqs 5.2, 5.3, and 5.4, using a nonlinear least-squares method extended to complex numbers. The fit (Figure 5) was obtained assuming that the diffusion coefficient is independent of concentration. This approximation is justified since $\Delta(H/M) = 0.065$ during the experiment. The average particle diameter of the "as-received" sample was found to be 50 μm from X-ray diffraction measurements. The average particle size of $LaNi_5$ is known to decrease along the first hydriding cycles down to ca. 5 μm. The experimental transfer function of Figure 5 was obtained after the first hydriding cycle, but the exact particle size was not measured. Data were therefore fitted assuming a particle diameter of 50 μm, and this yields an overestimated value of D (by a factor of 2 or 3). This points out a limitation of PIS analysis since several triplet values $\{r; D; dP/dC\}$ in eq 5.3 produce the same solution $Z_D{}^{sphere}(\omega)$. Another problem comes from the difficulty of accurately determing the experimental slope of the isotherm in the low concentration domain where hydrogen trapping is known to occur. When the exact average particle size of the sample and the slope of the isotherm at the measurement point are precisely known, only one value of D satisfactorily fits $Z(\omega)$ over the whole frequency range. Otherwise, erroneous values of D may be deduced from the fits. In Figure 5, the general agreement between measured and calculated spectra over the frequency domain supports the validity of the postulated two-step mechanism. From the fit, $R_s = 7 \times 10^9$ Pa·mol^{-1}·s and $D = 4 \times 10^{-10}$ cm^2·s^{-1} (298 K). This estimated value of D can be

compared to those obtained by other workers. Assuming that the bulk diffusion process was rds and neglecting surface effects, Tanaka et al. have measured the value of the concentration-independent diffusion coefficient D^* on defect-free and massive $LaNi_5$ samples, at infinite dilution, in the temperature range 353−463 K.[20] Extrapolation down to 298 K yields $D^* = 2.9 \times 10^{-9}$ $cm^2 \cdot s^{-1}$, a value ca. 1 order of magnitude higher that the one obtained in the present work on a defect-rich powdered sample. It should be noted that the mixed surface-diffusion rate control evidenced in the present work using PIS analysis may explain the difficulties encountered in ref 20 to fit experimental data at short and long time using a single diffusion-based rate equation. Ura et al. have measured D in massive β-$LaNi_5$−H particles using a microelectrode technique in 1 M KOH.[21] Using different particle sizes in the range 130−150 μm, they obtained an average value $\bar{D} = (4.3 \pm 1.9) \times 10^{-8}$ $cm^2 \cdot s^{-1}$ at 298 K which is one further decade higher than the value from Tanaka et al. in α-$LaNi_5$−H. Their results were found in good agreement with those obtained for the β phase by NMR measurements (1.3×10^{-8} $cm^2 \cdot s^{-1}$ [22,23]) and by QNS measurements (5×10^{-8} $cm^2 \cdot s^{-1}$ [24]). Such differences between α and β phases are known to exist in other intermetallic compounds and elemental metals such as Pd.[25] The low value of D estimated in the present work for the α phase can be attributed to the amount of defects induced by the first activation cycle. A detailed experimental study of the correlation between the value of D, the particle size distribution and the concentration of defects in the sample during the activation process is still needed.

6. PIS Analysis of Activation Process and Degradation Mechanism

Experimental impedance diagrams, similar in shape to those measured in solid solution domains, can be obtained in two-phase domains.[26] PIS analysis yields the value of the resistance associated with the first chemisorption step and the value of an average bulk diffusion coefficient. They can be measured as a function of different experimental parameters including H/M composition, temperature, etc. Thus, PIS provides a tool for investigating phase transformation mechanisms along the thermodynamic paths observed in hysteresis loops, as proposed elsewhere for electrochemical systems.[10] PIS can also be used to follow material activation and material degradation when absorption occurs in poison-containing hydrogen atmospheres, as discussed in the following.

6.1. IMC Activation Process. Activation process is the term used to describe the kinetics of hydrogen absorption/desorption during the first hydriding cyles. Most IMCs are brittle, and the action of hydrogen leads to powders of increasing surface area during the first hydriding cycles. Thus, the surface resistance related to the first chemisorption step decreases accordingly down to a constant value. Surface resistances measured during the two first cycles of the activation process of $LaNi_5$ are shown in Figure 6.

A first scan is made in the solid solution domain (from H/M = 0.0 to 0.7 and return) using 2.374 g of "as-received" $LaNi_5$ powder sample (plots 1 and 2). The surface resistance is significantly high during absorption and slightly lower during desorption. A significant rise is observed at the beginning of the plateau pressure where the hydride β phase begins to precipitate. Then, the sample is further activated by the combined action of pressure and temperature: a second scan (not represented here) is performed at 100 °C by transferring/withdrawing amounts of hydrogen from H/M = 0.0 to ca. 5.5 (precipitation of β phase) and return. Finally, the sample is cooled to room temperature and a third scan is performed in the solid solution domain after the first activation cycle (plots 3 and 4). A significant decrease of the surface resistance is observed: the activation process creates fresh IMC−H_2 interfaces (the material is pulverized during the precipitation of the β phase) where sorption proceeds faster. The decrease of the surface resistance during the hydriding process can be reasonably attributed to the increase in interface area or to the reduction of surface oxide layers yielding increased kinetic parameters. Thus, PIS provides a tool to separately measure surface and bulk rate contributions. It can be used to optimize activation procedures which should lead to low surface-resistance values without losses of sorption capacities.

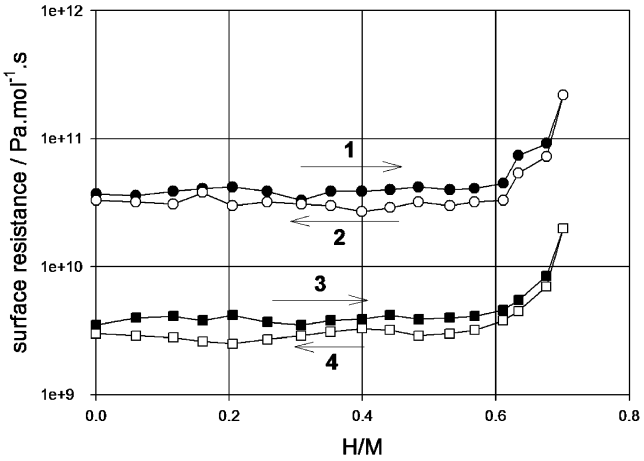

Figure 6. Experimental plots of the high-frequency semicircle of the transfer function vs composition for $LaNi_5$ at 298 K, in the solid solution domain: 1 and 2, absorption and desorption resistances measured on "as-received" material; 3 and 4, absorption and desorption resistances measured after a scan up to H/M = 5.5 in the two-phases domain.

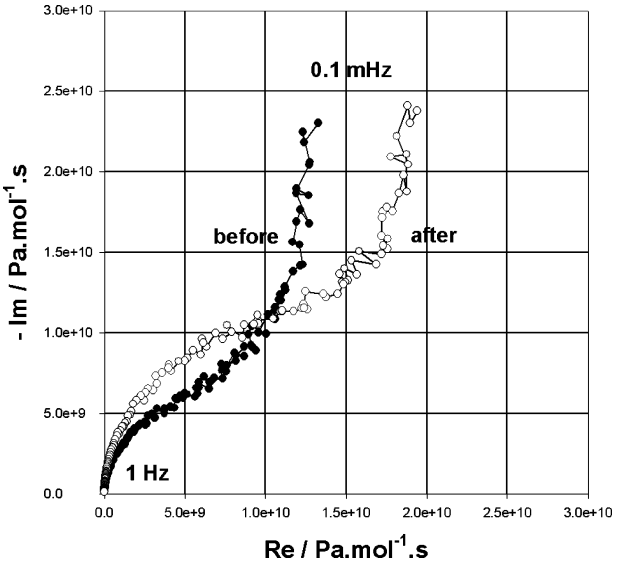

Figure 7. Pneumatochemical impedance diagrams recorded at 298 K on an activated $LaNi_5$ powder sample in the solid solution domain (H/M = 0.065) before (●) and after (○) exposure for 30 min to a 100 ppm oxygen containing H_2 atmosphere.

6.2. Degradation of Sorption Properties. Figure 7 shows the pneumatochemical impedance diagram measured at $T = 298$ K at the foot of the isotherm (H/M < 0.1), on a powdered and activated $LaNi_5$ sample before and after exposure to a 100 ppm oxygen containing H_2 atmosphere. Surface oxidation of the sample leads to high surface resistances and decreases the overall

kinetic ability of the sample to absorb/desorb hydrogen whereas bulk properties remain unchanged.

7. Conclusions and Perspectives

Pneumatochemical impedance spectroscopy (PIS) is the indirect transposition of electrochemical impedance spectroscopy (EIS) to solid−gas reactions. The practical conditions for obtaining experimental (i) pneumatic and (ii) pneumatochemical transfer functions using Sievert's-type gas distribution apparatus (SGDA) are discussed in this paper. The dynamic characteristics of individual pneumatic components (valves, volumic chambers) are obtained. It is shown that SGDA can be modeled using linear electrical analogies in which needle valves act as linear pneumatic resistances and volumic chambers as pneumatic capacitors. SGDA can be used to analyze the chemical mechanism associated with hydrogen absorption (desorption) by (from) metals and IMC in solid solution domain. It is shown that sorption is a two-step mechanism including (i) surface dissociative chemisorption of molecular hydrogen and (ii) diffusion-controlled bulk transport.

PIS provides a means for in situ and real-time mechanism investigation of IMC−H_2(g) systems. It can be used as a diagnostic tool for analyzing the degradation of sorption properties under cycling conditions or help in the research to synthesize new hydrogen storage materials with enhanced kinetics and storage capacities. Potentially, it offers the possibility of determining the mechanism rds for which rate improvement is needed. Evidence of surface limitations should lead to adequate surface treatments such as chemical modification or surface roughning to increase interfacial kinetics through better catalytic activity and higher surface area. Evidence of bulk transport limitations should lead research to chemical alloying in order to increase diffusion coefficient and lower internal strain generation during hydride formation. PIS can also detect shifts from one rds to another as a function of different experimental parameters including time, composition, and temperature and facilitates the modeling of kinetics data.

Potentially, the method can be used to investigate the kinetics of any IMC−H_2(g) system, including promising Mg-based compounds known to suffer from severe surface rate limitations[27] or the kinetics of hydrogen sorption on solids of large surface[28] including nanostructured carbon materials.[29−31] The method can also be extended to permeation experiments as well as to other solid−gas systems such as solid−O_2(g).

Acknowledgment. Financial support from Compagnie Européenne des Technologies de l'Hydrogène, Ecole Polytechnique, Palaiseau, France, is gratefully acknowledged.

References and Notes

(1) Dantzer, P.; Orgaz, E. *J. Less-Common Met.* **1989**, *147*, 27.
(2) Mintz, M. H.; Zeiri, Y. *J. Alloys Compd.* **1994**, *216*, 159.
(3) Caï, H.; Millet, P.; Dantzer, P. *J. Alloys Compd.* **1995**, *231*, 427.
(4) Martin, M.; Gommel, C.; Borkhart, C.; Fromm, E. *J. Alloys Compd.* **1996**, *238*, 193.
(5) Chou, K.-C.; Li, Q.; Lin, Q.; Jiand, L.-J.; Xu, K.-D. *Int. J. Hydrogen Energy* **2005**, *30*, 301.
(6) Wang, C. S.; Wang, X. H.; Lei, Y. Q.; Chen, C. P.; Wang, Q. D. *Int. J. Hydrogen Energy* **1996**, *21*, 471.
(7) Inomata, A.; Aoki, H.; Miura, T. *J. Alloys Compd.* **1998**, *278*, 103.
(8) Christian, J. *Theory of Transformations in Metals and Alloys*; Pergamon: Oxford, 1975.
(9) Castro, E. B.; Real, S. G.; Bonesi, A.; Visintin, A.; Triaca, W. E. *Electrochim. Acta* **2004**, *49*, 3879.
(10) Millet, P. *Electrochem. Commun.* **2005**, *7*, 40.
(11) Gray, E. Mac A. *J. Alloys Compd.* **1992**, *408*, 49.
(12) Flanagan, T. B.; Clewly, J. D. *J. Less-Common Met.* **1982**, *83*, 127.
(13) Dantzer, P.; Pons, M.; Guillot, A. *Z. Phys. Chemie* **1994**, *183*, 205.
(14) Bergland, G. D. A guided tour of the fast Fourier transform. *IEEE Spectrum* **1969**, July, 41.
(15) Press, W. H. *Numerical Recipes, the Art of Scientific Computing*; Cambridge University Press: Cambridge, 1986.
(16) Lim, C.; Pyun, S.-I. *Electrochim. Acta* **1993**, *38*, 2645.
(17) Jacobsen, T.; West, K. *Electrochim. Acta* **1995**, *40*, 255.
(18) Chen, J. S.; Diard, J.-P.; Durand, R.; Montella, C. *J. Electroanal. Chem.* **1996**, *406*, 1.
(19) Millet, P. *J. Alloys Compd.* In preparation
(20) Tanaka, S.; Clewley, J. D.; Flanagan, T. B. *J. Phys. Chem.* **1977**, *81*, 1684.
(21) Ura, H.; Nishina, T.; Uchida, I. *J. Electroanal. Chem.* **1995**, *396*, 169.
(22) Halstead, T. K. *J. Solid State Chem.* **1974**, *11*, 114.
(23) Bowman, R. C.; Gruen, D. M.; Mendelsohn, M. H. *J. Less-Common Met.* **1979**, *32*, 501.
(24) Richter, D.; Hempelmann, R. *J. Less-Common Met.* **1982**, *88*, 353.
(25) Millet, P.; Srour, M.; Faure, R.; Durand, R. *Electrochem. Commun.* **2001**, *3*, 478.
(26) Millet, P.; Dantzer, P, *J. Alloys Compd.* **2002**, *330*, 476.
(27) Song, Y.; Guo, Z. X.; Yang, R. *Phys. Rev. B* **2004**, *69*, 094205.
(28) Schlapbach, L.; Züttel, A. *Nature* **2001**, *414*, 353
(29) Ye, Y.; Ahn, C. C.; Witham, C.; Fultz, B.; Liu, J.; Rinzler, A. G.; Colbert, D.; Smith, K. A.; Smalley, R. E. *Appl. Phys. Lett.* **1999**, *74*, 2307.
(30) Browning, D. J.; Gerrard, M. L.; Lakeman, J. B.; Mellor, I. M.; Mortimer, R. J.; Turpin, M. C. *Nano Lett.* **2002**, *2*, 201.
(31) Deng, W.-Q.; Xu, X.; Goddard, W. A. *Phys. Rev. Lett.* **2004**, *92*, 166103.